Biochemistry and Biophysics Reports 39 (2024) 101787

Contents lists available at ScienceDirect

Biochemistry and Biophysics Reports

journal homepage: www.elsevier.com/locate/bbrep

Characterization of the tail current of Channelrhodopsin-2 variants

TiShang Zheng, HengQi Wei, CongJian Zhao *

Chongqing Engineering Research Center of Medical Electronics and Information Technology, School of Bioinformatics, Chongqing University of Posts and Telecommunications, 400065, Chongqing, PR China

ARTICLE INFO

Keywords:
Optogentics
Channelrhodopsin-2
Tail current
Stationary fluctuation analysis
Nonstationary fluctuation analysis
Photocycle

ABSTRACT

Our study focused on specific ChR2 variants, particularly those with the Step function Opsins (SFO) mutation at the D156-C128 gate. These are widely used in optogenetics due to their heightened sensitivity to light and bi-stable prolonged activation. However, in some ChR2 variants, specifically D156 mutants, a tail current occurs when continuous light exposure is stopped. We specifically examined the D156H-T159S ChR2 variant, which demonstrated a tail current that was somewhat responsive to light and voltage, with a single-channel current of around 9fA, similar to wt-ChR2 as determined by stationary noise analysis. To further investigate, we used nonstationary noise analysis in cell-attached patching mode, which revealed that the tail current's single-channel current falls within the same range as the peak current, albeit with mild contamination from adaptation and desensitization. This finding strongly supports the notion that a portion of the ChR2 molecules open or re-open at the end of illumination, leading to further membrane depolarization.

1. Introduction

Shortly after Channelrhodopsins-1 (ChR-1) [1], Channelrhodopsins-2 (ChR2) [2]) was cloned and confirmed to be a light-gated cation-ion channel, which was identified in 2001 and 2003 in oocytes and mammalian HEK cells, respectively. Since then, ChR2 has been used as an excitation tool for optogenetics [3–6] and vision restoration in blindness [7] due to photoreceptor cell loss in retinal pigmentosa (RP). Over two decades, researchers have developed dozens of ChR2 variants with improved light sensitivity, temporal and spatial resolution, and multiple spectra [8–11]. The DC (D156, C128) gate was proposed [12] and eventually confirmed to involve a water-mediated binding between C128 and D156 and to interact directly with the retinal Schiff base [13]. Some mutations to D156 or C128 dramatically slowed the closure kinetics [14–16]. Some DC mutations (mainly C128 mutations, including C128A and C128S) are called and referred to as step-function opsin (SFO) due to their bi-stable long activation under short illumination. It was generated by introducing a point mutation of ChR2 at position C128, including C128A ChR2, C128S ChR2, or C128T ChR2. Another variant, D156A ChR2, has a deactivation time scale of the order of minutes [16]. The combination of these two mutations resulted in a stabilized SFO-ChR2(C128S-D156A, SSFO), which has a stable step depolarization membrane potential of more than 30 min *in vitro* and *in vivo* [17,18]. The decay of the conducting state P520 is dramatically slowed down in C128T ChR2 [17,18] and D156E ChR2 [19]. Thus, The DC pair mutation slows the photocycle (transition from P520 to P480 state) with accumulating P520 [20].

After Frankenhaeuser first described the K^+ tail current from an isolated single fiber of the sciatic nerve of the frog *X. laevis* [21], tail currents were reported from most voltage-gated potassium channels (KV), sodium channels (NaV) [22], and calcium channels (CaV) [23]. NaV and CaV channels' inward tails are fast and masked by transients with larger capacitance. Therefore, the tail current of KV, especially the HERG (KCNH2) K^+ channel, has been thoroughly investigated [24]. In general, the tail current of the voltage-gated channel reflects the timing of channel closure initiated after stimuli termination. In addition, the inward tail current of ligand-gated *N*-methyl-D-aspartate receptor (NMDA receptor or NMDAR) has recently been reported [25–28]. The inward tail current of NMDAR suggests that the NMDA receptor channels accumulate in the open-blocked state. Thus, in addition to the tail current, which can affect the action potential and repetitive ring in target cells [24,29–34], the study of tail current will also facilitate the understanding of the mechanism of structural transformation.

Tail current is not often detectable in Xenopus oocytes or HEK 293 cells for wild-type channelrhodopsin-2 (*wt*-ChR2). Still, we found it is robust in some variants, e.g., point mutation D156 (D156H or D156C) alone or combined with other point mutations (Figs. 1 and 2, Supplementary Fig. 2). The first documented tail-like event is of C128S [14].

* Corresponding author.
E-mail addresses: zhaocongjian@cqupt.edu.cn, cj.zhao@yahoo.com (C. Zhao).

https://doi.org/10.1016/j.bbrep.2024.101787
Received 17 May 2024; Received in revised form 3 July 2024; Accepted 9 July 2024
Available online 16 July 2024

However, the tail current of ChR2 has yet to be well studied. We characterized the photocurrent of mutations of the DC pair of ChR2 under patch clamp and reported the tail current, a novel characteristic feature of ChR2.

2. Results

2.1. The tail current is induced upon the termination of continuous illumination in variants with D156H mutation

The light-induced photocurrents of ChR2 and the variants containing the D156H mutation were measured at 1000 ms light exposure. The photocurrent curve of *wt*-ChR2, T159C ChR2, and the T159S ChR2 variant show a characteristic peak current ($\mathbf{I_p}$) that inactivates to a steady-state current level ($\mathbf{I_{ss}}$) that exhibits rapid desensitization as a function of intensity (Fig. 1A–C), the parameters of photocurrent were extracted as Supplementary Fig. 1 A. In contrast, inward tail current responses were observed with D156H alone (Fig. 1 D) or with another site mutation (either T159C or T159S) (Fig. 1 E and F, respectively) upon cessation of continuous illumination, while the parameters of the tail current were extracted as illustration in Supplementary Fig. 1B. These data suggest that the tail current is attributed to the D156H mutant.

After reviewing literatures, the tail currents were visible in ChR2-XXL (D156C) [16,35,36], ChR2-XXM (D156H) [37,38], C128S [14], C128A, and D156A [16] expressed in Xenopus oocytes [14], C128T, D156A in HEK 239 T cell [39], C128T, and SFO including C128A and D156A in ND7/23 cells [40]. The tail current of ChR2 has yet to be well studied. Therefore, we focused on the D156 site mutants because the photocurrent is much lower in mutations of the C128*X* with a relatively faster photocycle (Supplementary Fig. 2 and [16]). In addition, the tail current is also detectable in variants with D156C, but it is not feasible to characterize because it recovers very slowly compared with D156H (Supplementary Fig. 2). Therefore, the tail current of ChR2 was mainly characterized using the double mutants D156H and T159S ChR2 (D156H-T159S ChR2**)**.

2.2. The tail current of the variants D156H-T159S ChR2 depends on the light intensity

The photocurrents of three ChR2 variants, including wt-ChR2, T159S ChR2, and D156H-T159S ChR2, were induced at six light intensities, as indicated in Fig. 2 A-C. The photocurrent curve of T159S is similar to the typical *wt*-ChR2 curve. The ratio of steady to peak current in ChR2 varies considerably between the variants [41]. Compared to *wt*-ChR2 (50-40 %) [41] and T159S ChR2 (50–60 %), D156H ChR2 exhibits much lower desensitization (about 5–10 %) (Fig. 2 D-I). The parameters of the above three variants are shown in Table 1 and Supplementary Tables 1–3. Neither *wt*-ChR2 nor T159S ChR2 contains a tail current. We then confirmed that the tail current is not an artificial effect, e.g., the external or internal electrical trigger by delivery light illumination by manually switching on or off the LED or light shutter of microscopy (data not shown). However, the tail current can be detected in most traces of the D156H-T159S double mutant, as indicated in Fig. 2. B–C and Supplementary Fig. 2. The amplitude of the tail currents shows an increasing proportion to the amplitude of the peak current (Fig. 2. F). This result indicates that the tail current depends on the light intensity. In addition, $\boldsymbol{\tau_{ON}}$ and the delay to peak ($\mathbf{D_{PEAK}}$, the delay from the onset of light exposure to the peak time) of D156H-T159S ChR2 negatively depend on light intensity. In contrast, the $\mathbf{D_{TAIL}}$ and $\boldsymbol{\tau_{ONT}}$ remain constant without relation to light intensity. This result suggests that more channels are responsible for increasing the tail current amplitude dependent on light intensity. However, the activation timing of these molecules is relatively constant, about in the 2–3 ms range.

2.3. The tail current of the variant D156H-T159S ChR2 is voltage-dependent

Using multiple voltage step protocol (Fig. 3 A), the raw and tail currents, subtracted from Iss traces, were plotted in Fig. 3 B–C. We investigated whether this tail current was related to a voltage (Fig. 3 B–C). Experimental measurements of the reversal potential of ChR2 are difficult due to the low current and poor signal-to-noise ratio around this point. In contrast, the ChR2 and most variants show strong inward rectification for peak and steady-state current at voltages above 0 mV [42,43]. The reversal potential of the peak and tail current of the

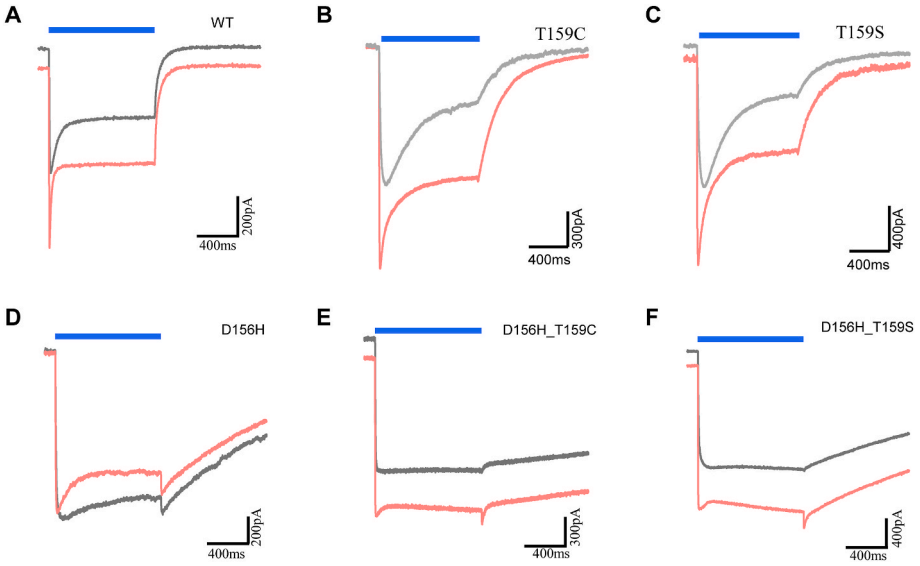

Fig. 1. Macroscopic photocurrent of channelrhodopsin-2 variants under whole-cell patch recording. Representative photocurrents of channelrhodopsin-2 variants, *wt*-ChR2 (**A**), T159C (**B**), T159C (**C**), D156H (**D**), D156H-T159C (**E**), and D156H-T159S (**F**) were induced by an LED (470 nm). Please note that the tail current was elicited after the termination of illumination in the variants with the D156H mutation but was not observed in *wt*-ChR2 and the T159 point mutations (T159C and T159S, respectively). The grey and the red photocurrent traces were induced at a light intensity of 1.21 and 14.2 mW/mm^2, respectively. (For interpretation of the references to colour in this figure legend, the reader is referred to the Web version of this article.)

D156H-T159S ChR2 variant shows a rightward shift at about +40.4 mV and +44.1 mV, respectively, in 137.93 mM mM $[Na^+]_o$ solution (Fig. 3 E, H) compared to *wt*-ChR2 is about +8 mV in 145 mM $[Na^+]_o$ (Fig. 3 D) [43]. The peak, steady-state, and tail currents respond to voltage non-linearly (Fig. 3H), while the $\mathbf{I_{Tail}/I_p}$ ratio is linear (Fig. 3 G). Thus, the amplitude of the tail current of D156H-T159S ChR2 is both light- and voltage-dependent.

2.4. The single-channel current of the D156H-T159S ChR2 was measured using a nonstationary noise analysis

The single-channel current of ChR2 is not feasible to measure using classical single-channel recording because of the small single-channel current (about the fA range). To estimate the unitary channel currents of the D156H-T159S ChR2 variant, we first measured the single channel current of ChR2 using stationary noise analysis [44,45]. Steady-state noise analysis revealed that the single channel current of D156H and T159S is approximately 9.2fA (Supplementary Fig. 3), which is in the same range as *wt*-ChR2 [44]. In this approach, only functional channels in the plasma membrane during the 120sec state-steady period are recorded post-illumination (Supplementary Fig. 3), mainly attributed to the conducting P^N520 and $P^{*N}520$ states [20]. Thus, the single channel current of the tail current is not feasible to measure using stationary noise analysis. Therefore, non-stationary noise analysis was performed using the previous method [43] with slight modifications. Since the rundown or adaptation of macroscopic photocurrent of ChR2s was served under whole-cell mode (data not shown). The noise analysis experiment was conducted in the cell-attached mode of the patch clamp with a 20 ms illumination duration and an interval of 20 s between two trials for *wt*-ChR2 and G224S ChR2, while an illumination duration of 500 ms and an interval of 22 s was applied for D156H-T159S ChR2. In this approach, only functional channels in the plasma membrane were considered during stimulation (Supplementary Fig. 4). The mean maximum response amplitudes of D156H-T159S ChR2 (−9 pA, n=14) were not significantly different in the transfected HEK cells (Fig. 4).

Variance (σ^2) due to the random channel noise was calculated from the trial-to-trial variance, which is accessible from the artifact introduced by rundown or adaptation (Fig. 4 D-F, Supplementary Fig. 4 A1-2) [46]. The variance against the mean of the peak current was plotted and fitted using the parabola equation $\sigma^2 = I_i - (I^2/N)$ (*wt*-ChR2 in Fig. 4 B). The ranges of estimated single-channel currents of *wt*-ChR2 (−0.0865 ±0.033 pA; n=7) (Fig. 4 A-C), which are similar to previously measured

Table 1
The kinetic characteristics of ChR2 variants at 7.94 mW/mm^2 light intensity.

	τ_{ON} (ms)	τ_{INACT} (ms)	τ_{ONT} (ms)	τ_{OFF}/τ_{TAIL} (ms)
***wt*-ChR2**	2.8 ± 2.63	19.94 ± 5.56	Not appliable	30.54 ± 11.13
T159S	3.82 ± 1.49	196.61 ± 29.44	Not appliable	272.33 ± 20.93
D156H and T159S	2.82 ± 1.06	38.26 ± 12.57	3.16 ± 1.36	8132.26 ± 4594.35

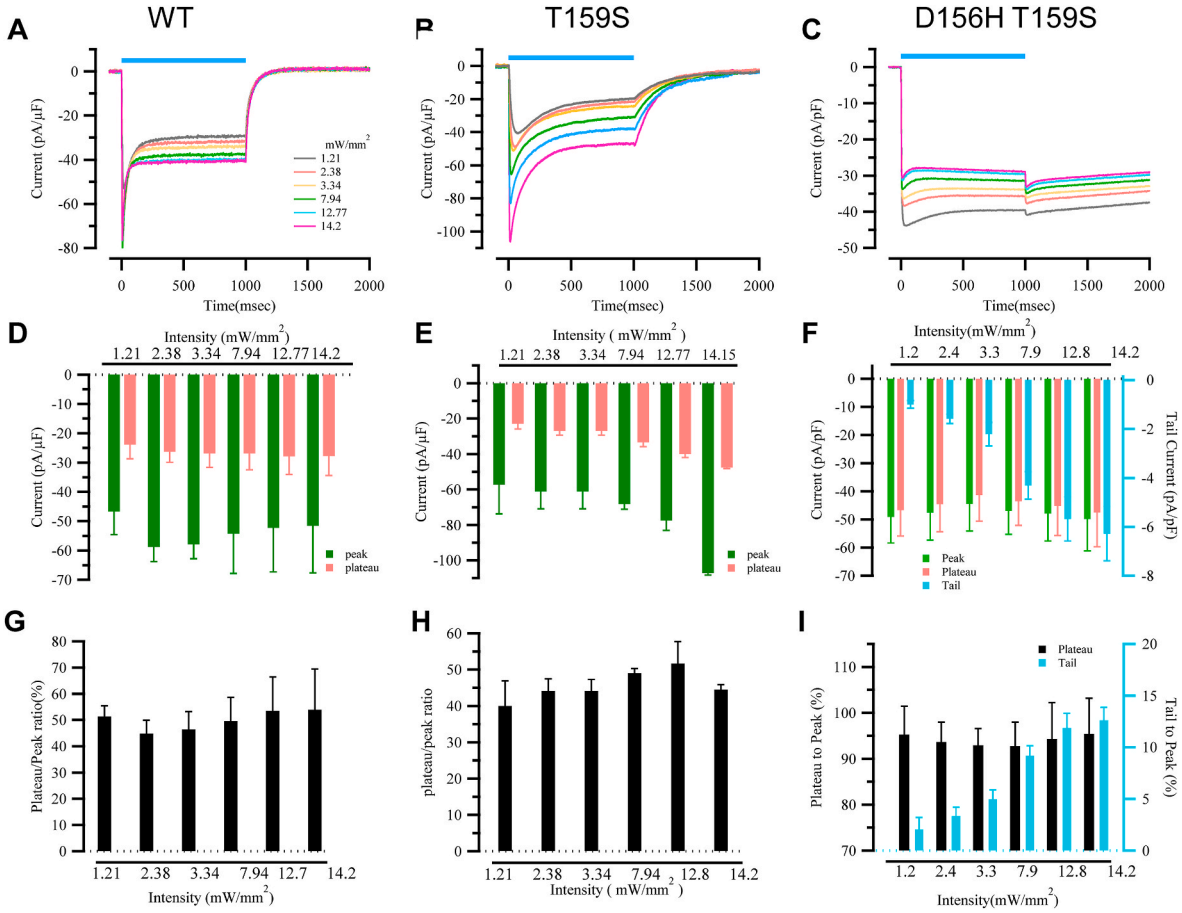

Fig. 2. Kinetic properties of ChR2 variants at different light densities. Representative photocurrents of channelrhodopsin-2 variants induced by different light intensities (1.21, 2.38, 3.34, 7.97, 12.77, and 14.2 mW/mm^2, respectively), *wt*-ChR2 (**A**), T159S ChR2 (**B**) and D156H-T159S ChR2 (**C**). The tail current of the D156H-T159S ChR2 variant can be observed in each trace induced at different light intensities. The amplitude of the peak and plateau currents were plotted in the histogram, *wt*-ChR2, n=5 (**D**), T159S ChR2 n=5 (**E**), and D156H-T159S ChR2, n=4 (**F**). The relationship between the amplitude of the plateau ($\mathbf{I_{ss}}$) or tail current and the peak currents was plotted in *wt*-ChR2 (**G**), T159S ChR2 (**H**), and D156H-T159S ChR2 (**I**).

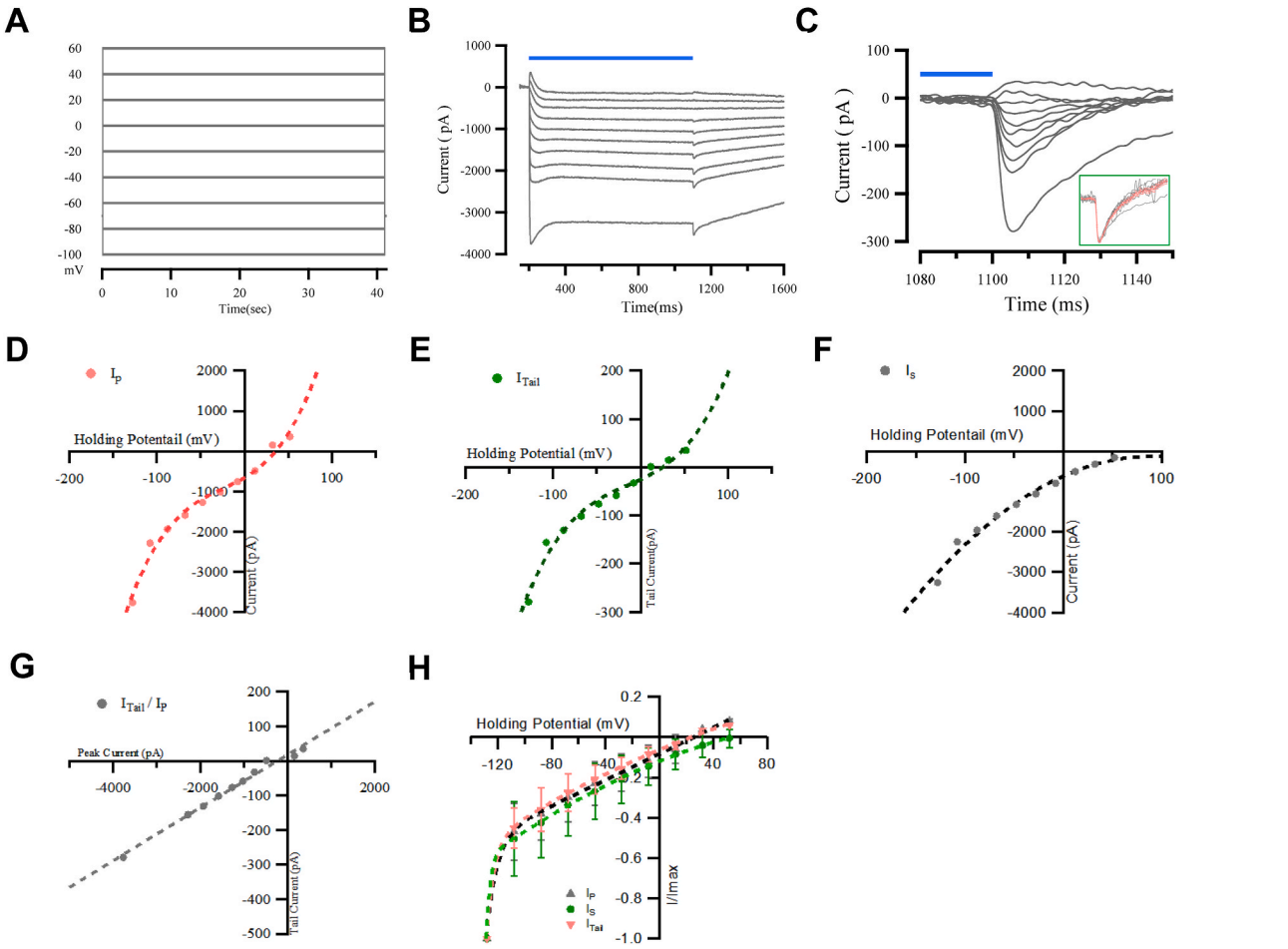

Fig. 3. Kinetic properties of the D156H-T159S ChR2 variant for the voltage protocol. **(A)** The voltage protocol was performed with a varying holding potential from −120mV to +60 mV in 20 ms steps. **(B)** The macroscopic photocurrent of the D156H-T159S ChR2 variant was induced by a 1000 ms 7.97 mW/mm^2 light from 470 nm LED under a voltage-dependent protocol with at least 40 s recovery. Note that the first trace with the largest amplitude is held at −120mV. The tail current traces after subtraction of $\mathbf{I_{ss}}$ were shown in **(C).** The negative tail current traces were normalized and recorded as **Inset**, showing that these traces' on and off kinetics are in the same range. The I–V curves were plotted in **(D-F)** ($\mathbf{I_p}$, $\mathbf{I_{ss}}$, $\mathbf{I_{TAIL}}$ respectively), and I/Imax against voltage and Boltzmann function fitting were plotted in **(H,** n=4). The relationship between $\mathbf{I_{TAIL}}$ and $\mathbf{I_p}$ was plotted in **(G).**

parameters [43]. The representative traces of a set recording were illustrated in a two-dimensional plot in (Fig. 4 D) The variance σ^2 was calculated by subtracting sequentially (Supplementary Fig. 4 B) or trial to trial difference (Fig. 4 E, Supplementary Fig. 4C) for further determination of variance σ^2 in (Fig. 4 G). While G224S ChR2 (−0.1200 ±0.254 pA; n=18) and D156H-T159S ChR2 (−0.1701±0.0731 pA; n=13) (Fig. 4C). To estimate the single-channel current of the tail current of D156H-T159S ChR2, the mean and variance of the beginning and end of the light (±10 ms from the center of the time of light on or off) of traces were calculated, respectively. The mean-variance plot and least-squares plot of D156H-T159S ChR2 obtained from the beginning and end of the light coordinate the peak current and tail current in Fig. 4 G-I. The estimated single channel currents of D156H-T159S ChR2: peak current (−0.1793±0.0831 pA, n=13) and tail current, (−0.1750 ±0.0773 pA, n=13) (Fig. 4 J). Moreover, the relationship between the single channel current of the tail current and the peak current (Fig. 4 K and L) showed that the single channel current of the tail current is somehow related to the peak. Our data support the notion that the opening or re-open of a proportion of the channel causes the tail current at the termination of illumination since the single channel current of the tail current is not alerted compared with the peak current, suggesting that a transition from a non-conducting state to conducting state or from a low efficient conducting state to high efficient conducting state is attributed to the tail current. Berndt et al. proposed that the transient accumulation of the conducting P520 state due to relatively slow decay leads to the accumulated P390 state due to equilibrium to the p520 state, which could give rise to the small peak observed at light-off in C128S [14]. The possible mechanism will be discussed in detail lately.

2.5. The tail current of D156H-T159S ChR2 variants further depolarizes the membrane potential

The membrane potential caused by the tail current of the ChR2 variants was monitored in whole-cell current-clamp mode (Fig. 5. A and B). There is an additional depolarization (about 1–2 mV change from relative constant membrane potential coordinated to the steady current of ChR2) induced by the tail current at the termination of light exposure (Fig. 5. A and B). The change can be appreciated in differentiated membrane potential, current, and against plot (Fig. 5. D, E, and C., respectively). This suggests that additional membrane depolarization caused by tail current may induce additional action potentials in the target cell depending on the intrinsic electrophysiological properties of the cell and circumstance.

3. Discussion

Tail current was visible, but without proper documentary, in ChR2-XXL (D156C) [16,35,36], ChR2-XXM (D156H) [37,38], C128S [14],

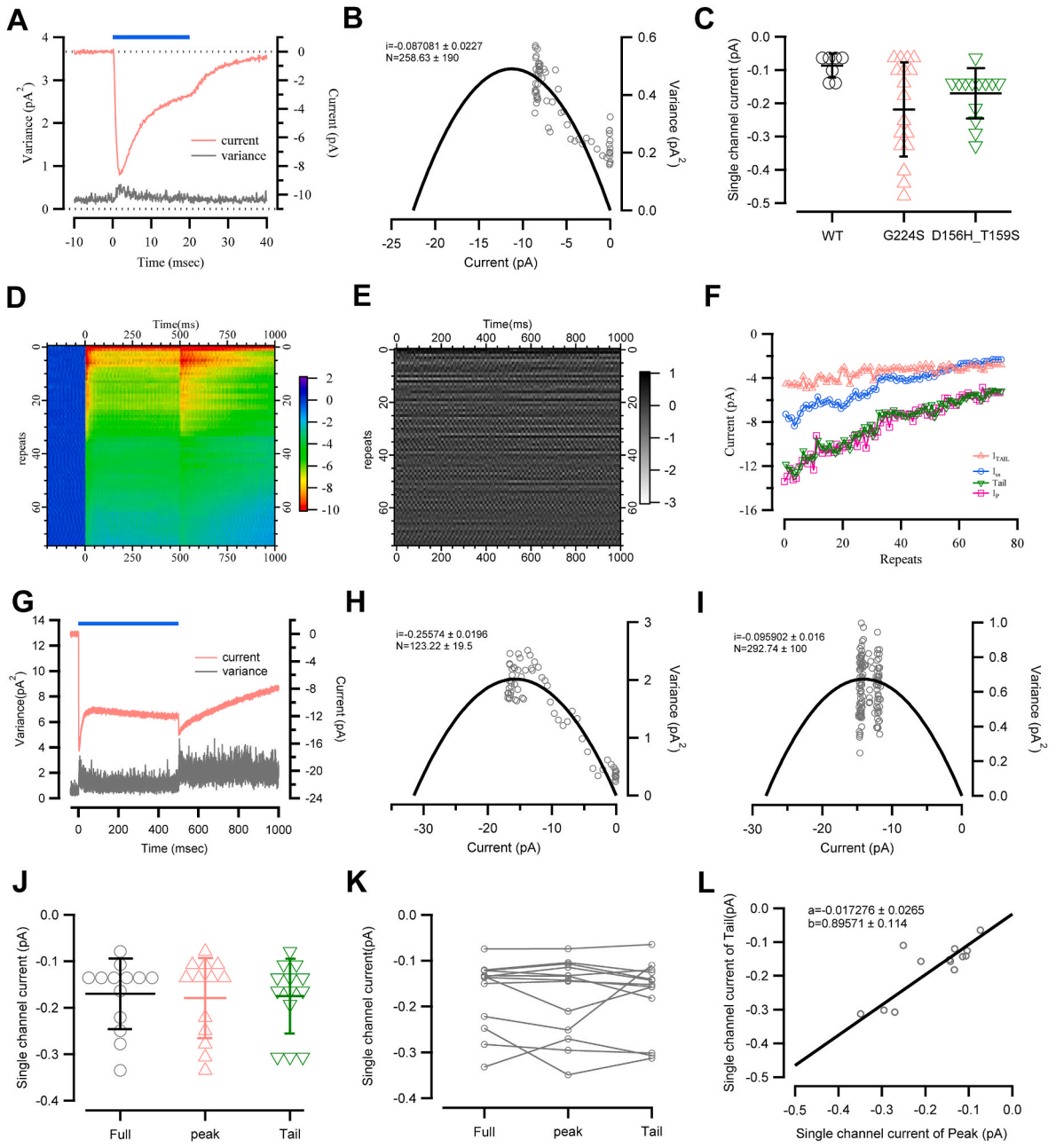

Fig. 4. The single channel current of the ChR2 variants estimated by non-stationary fluctuation analysis. Non-stationary fluctuation analysis of ChR2, G224S ChR2, and D156H-T159S variant was performed using a patch-clamp setup in cell-attached mode. (**A**) An example of non-stationary fluctuation analysis of *wt*-ChR2. The mean (red curve) and variance (grey curve) of *wt*-ChR2 were determined from 75 pulses of 470 nm light with a duration of 20 ms and 20 s of recovery. (**B**) The mean-variance plot and the least-squares fitted curve of *wt*-ChR2 were obtained from the slope of the response. (**C**) The estimated single-channel currents of *wt*-ChR2 (−0.0865±0.033 pA; n=7), the G224S variant (−0.1200±0.254 pA; n=18) and the D156H-T159S ChR2 variant (−0.1914±0.104 pA; n=14). Seventy-five repeating recordings with 500 ms light illumination and 22-s intervals were applied to D156H-T159S ChR2. The representative traces of a set recording were illustrated in a two-dimensional matrix in (**D**). The variance σ2 was calculated by trial-to-trial difference (**E**) and calculated the variance presented in (**G**, grey curve). **(F) I_p, I_{ss},** and **I_{TAIL}** were plotted against repeat numbers. (**G**) An example of a non-stationary fluctuation analysis of the D156H-T159S ChR2 variant. This variant's mean (red curve) and variance (grey curve) were obtained from 75 pulses of 470 nm light with a duration of 500 ms and 20 s of recovery. The mean-variance plot and the least-squares fitted curve of the D156H-T159S ChR2 variant obtained from the onset and termination of light exposure coordinate to peak current and tail current in (**H**) and (**I**), respectively. (**J**) The estimated single channel currents of D156H-T159S ChR2 variant: Full trace, −0.1701±0.0731 pA, n=13; Peak current, −0.1793±0.0831 pA, n=13; and tail, −0.1793±0.0831 pA, n=13. The single cell current from each measurement (cell) was plotted in (**K**), while the relationship between the single channel current of the tail current and peak current was plotted in (**L**). (For interpretation of the references to colour in this figure legend, the reader is referred to the Web version of this article.)

C128A, and D156A [16] expressed in Xenopus oocytes, C128T [39], D156A [16] in HEK 239 T cell, but sometimes not in oocytes. We demonstrated that the DC pair mutations, including D156H, D156C, and C128T, are attributed to the tail current. The tail current of D156H-T159S ChR2 is related to the holding voltage and light intensity. However, the presence of the tail current in ChR2 variants expressed in oocytes, or HEK 239 T cells, varies across studies. The investigation of two types of cells on the tail current of ChR2 is still needed.

Using the stationary and nonstationary noise analysis, we estimated the single-channel current of D156H-T159S ChR2. The single-channel

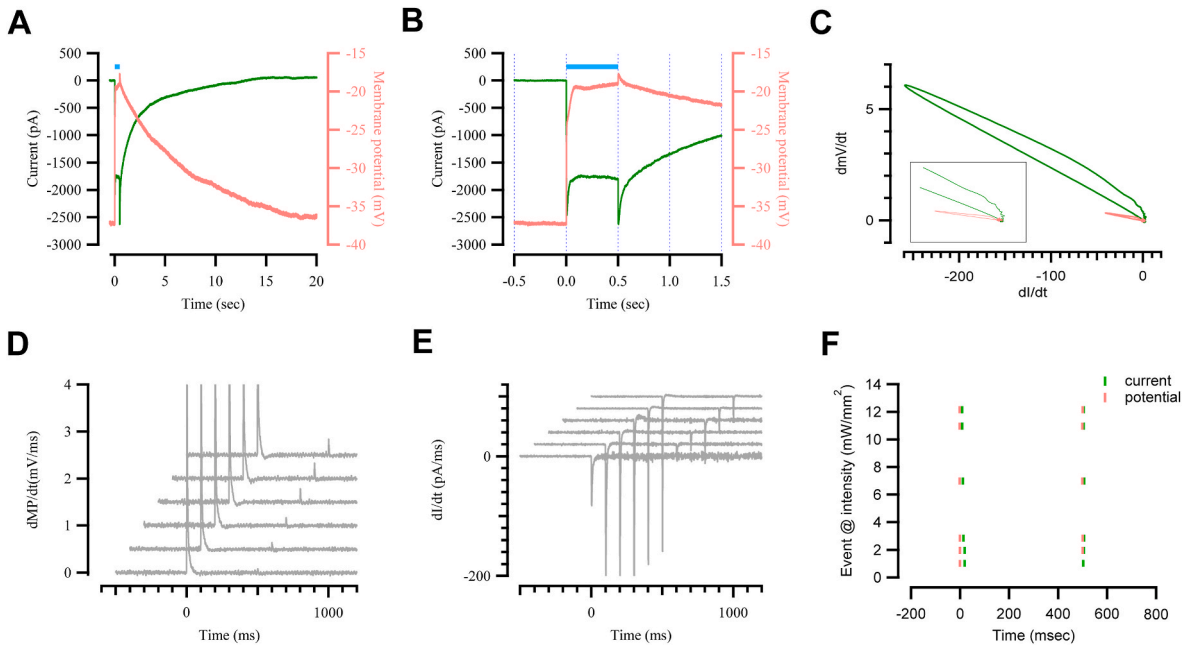

Fig. 5. The tail current induces a transient increase in membrane potential. Photocurrent and membrane potential induced by different light intensities were recorded with the current clamp for the whole cell and the voltage clamp at 3-min intervals (**A and B**). It demonstrated that the tail current triggered a further depolarization of the membrane potential at the end of light exposure. The differentiated membrane potential and inward current were plotted in **D and E,** respectively. The detailed change is shown in the relationship between the differentiation of the membrane potential and the current in (**C**). Please note that the membrane potential and current change transiently and rapidly at the beginning and end of light exposure, as demonstrated in the raster plot (**F**).

current of the stationary phase of D156H-T159S ChR2 determined by the stationary method is about −9.2 fA. Thus, this variant has a similar range of single-channel current compared to *wt*-ChR2 (−7.5±0.6 fA) [44]. However, it only reflects the single channel current of the extended stationary phase of ChR2s. Therefore, a non-stationary noise analysis was performed to overcome this difficulty. Considering that the ChR2 variants containing the D156H mutation recover more slowly, the cell-attached mode patch clamp was conducted to calculate the trial-to-trial variance to minimize adaptation and desensitization. The estimated single-channel currents of D156H-T159S ChR2 are peak current, −0.1793±0.0831 pA, and tail current, −0.1750±0.0773 pA, respectively. The single current yielded from the nonstationary noise analysis was about 20 folds the parameter obtained from the stationary noise analysis because of contamination of adaptation and channel desensitization (Fig. 4 D and F). However, it demonstrates that the single-channel current of the tail current is in the same range as the peak current. In addition, in the analysis of non-stationary noise, the light dependence of σ^2 was fitted according to the parabola function $\sigma^2 = Ii - (I^2/N)$, which allows estimating the number N of active ChR2 molecules within the cell membrane (≈43–77 ChR2/μm^2). This number is slightly smaller than that obtained by directly counting particles in the plasma membrane using electron microscopy and the parameter measured under steady-state noise analysis [44,47] since patched cells with lower expression of ChR2 variants were selected for nonstationary noise analysis experiments.

Our study delves into the unique behavior of ChR2 variants 'tail current.' The tail current of a voltage-dependent channel is a deactivated current that emerges after prior and sufficient activation. In contrast to the classical tail current of voltage-dependent channels, the tail current in ChR2 variants is particularly intriguing as it reflects the timing of channel opening or re-opening, similar to the inward tail current of NMDAR accumulating in the open-blocked state. This timing is initiated after the stimuli are terminated and is primarily influenced by light intensity and voltage. Our research challenges the conventional understanding of the ChR2 photocycle. The single unbranched photocycle, we found, is insufficient to explain photocurrent changes during extended light application. Therefore, we provide a possible mechanism on the tail current of ChR2s using a parallel two-cycle model comprising two closed (C1 and C2) and two open (O1 and O2) states [20]. These states are populated differently in the dark and during repetitive or continuous illumination, leading to a more comprehensive understanding of the ChR2 photocycle [20]. After light activation, the photocurrent of ChR2s exhibits an initial peak that rapidly decreases to a lower but stable level. This inactivation effect is attributed to the branched photocycle of ChR2, as illustrated in **the graphic abstract**. Moreover, the $P^{*N}520$ accumulates due to its slow decay and contributes to the stationary photocurrent under continuous illumination [20].

In variants with no prominent tail currents, under continuous illumination, accumulation of the P390a and P390b are minor due to the fast decay of P^N520. Meanwhile, the $P^{*N}520$ contributes to the steady-state progress directly to D470 or P480 non-conducting states [20,48]. Inactivation of *wt*-ChR2 is about 40–50 % of the peak amplitude depending on light intensity and previous illumination experience upon relatively continuous illumination (Figs. 1 and 2), indicating that probably 40–50 % of molecules participate in *syn*-photocycle actively [20]. In variants with prominent tail currents, the accumulating conducting state P520 of DC pair variants due to a rather slow decay and long lifespan leads to the accumulation of P390 proposed [14], which was confirmed lately in the nine-state single photocycle model of ChR2-C128T [18]. Moreover the decay conducting P520 state of *wt*, C128T, C128A, D156A ChR2 is 8.5 ms, 29s, 30s, 300s respectively [16]. The branched unifying photocycle model for light adaptation and temporal evolution was proposed latterly [20]. In this model, the late P390b and P^N520 contribute to the ion conductance of the open channel [16,18,49]. Accumulation of the conducting P^N520 state of D156H-T159S ChR2 due to relatively slow decay leads to accumulation of the small conducting P390b state and, therefore, may lead to accumulation of non-conducting state P390a due to P390b or P390a equilibrium with the accumulation of the conducting $P520^N$. Therefore, the transition of the accumulated P390b to P^N520, or P390a to P390b, then to P^N520, is attributed to the tail current on the termination of continuous illumination. Furthermore, the onset time of the tail current is about 2.5 ms,

which is in the same range as the parameter of the peak current (2.5 ms). In comparison, the transition from P390 to P520 (0.33 ms, 3.7 ms for C128T, C128A respectively) is identical to the kinetics in wild-type ChR2 (1.8 ms) [16].

Moreover, D156H ChR2 and D156H-T159S ChR2 inactivation are about 5–10 % of peak amplitude, much less than 40 % of *wt*-ChR2 (Figs. 1 and 2), upon relatively continuous illumination. The tail current is noticeable when the duration of the light stimulus is more than 20 ms (data is not shown and [16]). In contrast to the inactivation of variants without tail current, the inactivation is attributed from $P^{*N}520$; the actual inactivation of variants with tail current accounting from $P^{*N}520$ should be only small fraction since $\mathbf{I_{TAIL}}$ is about 90 % the decrease current from $\mathbf{I_p}$ to $\mathbf{I_{ss}}$ ($\mathbf{I_p}$-$\mathbf{I_{ss}}$) under continuous illumination (Supplementary Fig. 4 F), suggesting decrease current under continuous illumination is primarily contributed from accumulated nonconducting P390a state. However, the subtle accumulation of P390b and/or P390a state measurement and computation simulation upon long-term illumination are needed to address this question.

Finally, the tail current at the termination of light exposure causes an additional depolarization (about 1–2 mV change), which may induce extra action potential if a variant is expressed in the excitatory cell, for instance, neuron or muscle cell. The continuous illumination depolarized the membrane potential with an additional spike at the termination of illumination in C128S ChR2 expressing cells of the Drosophila horizontal plate lobula system, suggesting that C128S ChR2 may contain a tail current [50]. D156H ChR2 (XXM) showed enhanced Na^+ and Ca^{2+} conductance [36]. Compared to *wt*-ChR2, the duration of the tail current is usually 2–3 ms; the integrated Ca^{2+} influx during the tail current may evoke intracellular calcium signaling besides inducing additional action potentials. Moreover, the Ca^{2+} current of the tail current in cardiac myocytes can also trigger sarcoplasmic reticulum (SR) Ca^{2+} release [51]. Transient increase of Ca^{2+} may increase synaptic transmission if the D156H ChR2 mutant is expressed in the presynaptic compartment. Thus, depending on the intrinsic electrical properties and physiological conditions of the target neuron, the tail current of the ChR2 variants may elicit more action potentials. This also suggests that the tail current may affect the target cells' action potential and repetitive firing [24].

4. Materials and methods

4.1. DNA constructs

The ChR2 mutations at the D156, T159, and E123 sites were created by PCR and recombination strategy (KOD one master Mix, TOYOBO, Japan for PCR; Seamless Assembly Cloning kit, Clone Smarter, USA) and then verified by DNA sequencing, which is provided by Genmedicn Biopharma Inc. (Nanjing, China).

4.2. HEK cell culture, DNA transfection

HEK-293 T cells were maintained in Advanced Dulbecco's Minimum Essential Medium (Bio-Channel, China) supplemented with 5 % fetal bovine serum (Bio-Channel, China), 100 units/ml penicillin G, and 100 μg/mL streptomycin at 37 °C in a humidified 5 % CO2 atmosphere. In preparation for DNA transfection, the cells were seeded in 16-mm glass coverslip (Menzel Glaser, Braunschweig, Germany) and then transfected with *wt*-ChR2 or ChR2s mutant using Lipofectamine 2000 (Life Technologies). All-trans-retinal (1 μM) was added to the culture media during DNA transfection [52]. Patch-clamp recordings were performed two days after DNA transfection.

4.3. Patch clamp recording

Macroscopic photocurrent recordings of ChR2s with patch electrodes in the whole-cell configuration were acquired using standard procedures at room temperature (22 °C) with either epatch (elements, Italy) or EPC-10 amplifier and PULSE software (Heka Electronik, Lambrecht/Pfalz, Germany). The resistance of the electrode was 5–8 MΩ. The series resistance ranged from 8 to 20 MΩ. Cell capacitance was canceled using the acquiring software. Recordings were performed in Hank's balanced salt solution containing (in mM): 138 NaCl, 1 NaHCO3, 0.3 Na2HPO4, 5 KCl, 0.3 KH2PO4, 1.25 CaCl2, 0.5 MgSO4, 0.5 MgCl2, 5 HEPES, 22.2 glucose (Beyotime Biotechnology, China), and the pH was adjusted to 7.2 using 0.3 M NaOH. All-trans-retinal (1 μM) was added to the recording solution [52]. The electrode solution contained (in mM): 110 Cs-Methanesulfonate, 30 TE A-Cl, 2 MgCl2, 0.1 CaCl2, 10 EGTA, and 10 HEPES (Sigma, Germany). The pH was adjusted to 7.25 using CsOH. Voltage errors were minimized using 70–80 % series resistance compensation. Membrane potentials were corrected for liquid junction potential (~9.94 mV at 22 °C).

Most stationary or nonstationary noise analysis was recorded in cell-attached or whole-cell mode. Hank's balanced salt solution was used as the patching pipette for cell-attached mode. If whole-cell mode were to be performed, the 110 mM Cs-Methanesulfonate internal solution would be used, as mentioned above. For stationary fluctuation analysis [43, 53], transfected HEK cells were recorded without or with stimulation with 120 s of light with 120-s intervals at a given light intensity or holding voltage. For nonstationary fluctuation analysis [40], transfected HEK cells were stimulated with 75 successive pulses (20 ms duration) of light at 22-s intervals.

4.4. Light stimulation

Light stimulation was provided by a custom-made light-emitting diode (LED) system (Thorlab, USA) triggered by a patch clamp amplifier. The light beam was passed through a GFP filter set (BP 470/40, dichroic mirror FT 495). Various light intensities were achieved by adjusting the power supplier's input current; the beam's light intensities through optical len were measured using a light power meter (Thorlab, USA). The shutting down of light stimulation for noise analysis was achieved by manually switching off the power supplier. Light stimuli were coupled to the microscope and through an air lens with a numerical aperture of 0.6 (Nikon).

4.5. Data analysis

4.5.1. For light stimulation and voltage protocol recording

Eight parameters were defined to characterize the ChR2 photocurrent (Supplementary Fig. 1A). Five parameters for the photocurrent without tail current: amplitude parameters, namely peak current, $\mathbf{I_p}$, and steady-state current, $\mathbf{I_{ss}}$; three kinetic measures, the time constant of activation, $\boldsymbol{\tau_{ON}}$, of deactivation, $\boldsymbol{\tau_{OFF}}$, and inactivation, $\boldsymbol{\tau_{INACT}}$. For the D156H-T159S ChR2 mutations, another three tail current parameters were defined: the peak of the tail current, $\mathbf{I_{TAIL}}$; the time constant of tail current activation, $\boldsymbol{\tau_{ONT}}$; the time constant of deactivation, $\boldsymbol{\tau_{TAIL}}$, replacing $\boldsymbol{\tau_{OFF}}$, as shown in Supplementary Fig. 1. B.

4.5.2. For stationary fluctuation analysis

Recordings of the stationary current during prolonged illumination at varied light intensities (120 s) at −70 mV holding potential and 20–25 °C were used to estimate the unitary channel current of the underlying channel (2 kHz low-pass Bessel filter; sampling rate 20 kHz) [44]. Recordings were collected without (control) and with illumination. Data were transformed into files in either Igor Pro or Clampfit format. Noise analysis power spectral densities were calculated by a fast Fourier Transform (FFT) routine implemented in the Clampfit 10.0 software (spectral resolution: 0.076 Hz). Spectra were obtained by averaging individual spectra with illumination (channel noise; 2 measurements on the same cell; Supplementary Fig. 3 B red) and without illumination (background noise; 2 measurements on the same cell; Supplementary Fig 3. A and B black). For difference spectra, the background noise was subtracted from the channel noise spectrum

(Supplementary Fig 3. C). The difference spectrum was fitted between 1 Hz and 1 kHz with a single Lorentzian function ($S(f) = S_0/\left(1 + \left(f / f_c\right)^2\right.$, Eq. 1) and the variance was determined ($\sigma^2 = \frac{\pi \bullet f_c \bullet S(0)}{2}$, Eq. 2) the single channel parameters were determined ($i = \frac{\sigma^2}{I \bullet (1-P_0)}$, Eq. 3 and $(1 - P_0) = \frac{1}{2\pi \bullet f_c \bullet \tau_{off}}$), Eq. 4). Data analysis was performed with Clampfit 10.0 (Axon Laboratories) or Igor Pro (WaveMetrics, USA).

4.5.3. For nonstationary fluctuation analysis

Transfected HEK cells were performed either with a cell-attached or whole-cell mode patch clamp and stimulated with 50–75 pulses (20 ms duration) of light at 22-s intervals [43,53]. The mean response and trial-to-trial variance for each cell were calculated and fit with the parabola function ($\sigma^2 = I_i - \frac{I^2}{N}$, Eq.5) using Igor Pro (WaveMetrics, USA) as indicated.

CRediT authorship contribution statement

TiShang Zheng: Writing – original draft, Validation, Methodology, Formal analysis, Data curation. **HengQi Wei:** Methodology, Investigation, Data curation. **CongJian Zhao:** Writing – review & editing, Writing – original draft, Visualization, Validation, Supervision, Software, Resources, Project administration, Methodology, Investigation, Funding acquisition, Formal analysis, Data curation, Conceptualization.

Declaration of competing interest

The authors declare the following financial interests/personal relationships which may be considered as potential competing interests: CongJian Zhao reports financial support was provided by Natural Science Foundation Project of Chongqing. CongJian Zhao reports financial support and equipment, drugs, or supplies were provided by Fundamental Research Funds for the Chongqing University of Posts and Telecommunications. If there are other authors, they declare that they have no known competing financial interests or personal relationships that could have appeared to influence the work reported in this paper.

Acknowledgments

This work was supported by the Natural Science Foundation of Chongqing (2023NSCQ-LZX0050) and Fundamental Research Funds for the Chongqing University of Posts and Telecommunications (E011A2022316).

Appendix A. Supplementary data

Supplementary data to this article can be found online at https://doi.org/10.1016/j.bbrep.2024.101787.

References

[1] G. Nagel, et al., Channelrhodopsin-1: a light-gated proton channel in green algae, Science 296 (5577) (2002) 2395–2398.
[2] G. Nagel, et al., Channelrhodopsin-2, a directly light-gated cation-selective membrane channel, Proc. Natl. Acad. Sci. U.S.A. 100 (24) (2003) 13940–13945.
[3] E.S. Boyden, et al., Millisecond-timescale, genetically targeted optical control of neural activity, Nat. Neurosci. 8 (9) (2005) 1263–1268.
[4] T. Ishizuka, et al., Kinetic evaluation of photosensitivity in genetically engineered neurons expressing green algae light-gated channels, Neurosci. Res. 54 (2) (2006) 85–94.
[5] X. Li, et al., Fast noninvasive activation and inhibition of neural and network activity by vertebrate rhodopsin and green algae channelrhodopsin, Proc. Natl. Acad. Sci. U.S.A. 102 (49) (2005) 17816–17821.
[6] G. Nagel, et al., Light activation of channelrhodopsin-2 in excitable cells of Caenorhabditis elegans triggers rapid behavioral responses, Curr. Biol. 15 (24) (2005) 2279–2284.
[7] A. Bi, et al., Ectopic expression of a microbial-type rhodopsin restores visual responses in mice with photoreceptor degeneration, Neuron 50 (1) (2006) 23–33.
[8] S. Beck, et al., Synthetic light-activated ion channels for optogenetic activation and inhibition, Front. Neurosci. 12 (2018) 643.
[9] J.Y. Lin, A user's guide to channelrhodopsin variants: features, limitations and future developments, Exp. Physiol. 96 (1) (2011) 19–25.
[10] H.E. Kato, Structure-function relationship of channelrhodopsins, Adv. Exp. Med. Biol. 1293 (2021) 35–53.
[11] J. Wietek, M. Prigge, Enhancing channelrhodopsins: an overview, Methods Mol. Biol. 1408 (2016) 141–165.
[12] M. Nack, et al., The DC gate in Channelrhodopsin-2: crucial hydrogen bonding interaction between C128 and D156, Photochem. Photobiol. Sci. 9 (2) (2010) 194–198.
[13] O. Volkov, et al., Structural insights into ion conduction by channelrhodopsin 2, Science 358 (6366) (2017).
[14] A. Berndt, et al., Bi-stable neural state switches, Nat. Neurosci. 12 (2) (2009) 229–234.
[15] I. Radu, et al., Conformational changes of channelrhodopsin-2, J. Am. Chem. Soc. 131 (21) (2009) 7313–7319.
[16] C. Bamann, et al., Structural guidance of the photocycle of channelrhodopsin-2 by an interhelical hydrogen bond, Biochemistry 49 (2) (2010) 267–278.
[17] S. Bruun, et al., The chromophore structure of the long-lived intermediate of the C128T channelrhodopsin-2 variant, FEBS Lett. 585 (24) (2011) 3998–4001.
[18] K. Stehfest, et al., The branched photocycle of the slow-cycling channelrhodopsin-2 mutant C128T, J. Mol. Biol. 398 (5) (2010) 690–702.
[19] V.A. Lorenz-Fonfria, et al., Transient protonation changes in channelrhodopsin-2 and their relevance to channel gating, Proc. Natl. Acad. Sci. U.S.A. 110 (14) (2013) E1273–E1281.
[20] J. Kuhne, et al., Unifying photocycle model for light adaptation and temporal evolution of cation conductance in channelrhodopsin-2, Proc. Natl. Acad. Sci. U.S.A. 116 (19) (2019) 9380–9389.
[21] B. Frankenhaeuser, Instantaneous potassium currents in myelinated nerve fibers of Xenopus laevis, J. Physiol. 160 (1) (1962) 46–53.
[22] D.G. Wustenberg, et al., Current- and voltage-clamp recordings and computer simulations of Kenyon cells in the honeybee, J. Neurophysiol. 92 (4) (2004) 2589–2603.
[23] T.M. Curtis, R. Williamson, M.H. Depledge, Voltage activated currents in cardiac myocytes of the blue mussel, Mytilus edulis, Comp. Biochem. Physiol. Mol. Integr. Physiol. 124 (2) (1999) 231–241.
[24] S.A. Kodirov, Tale of tail current, Prog. Biophys. Mol. Biol. 150 (2020) 78–97.
[25] M. Benveniste, M.L. Mayer, Trapping of glutamate and glycine during open channel block of rat hippocampal neuron NMDA receptors by 9-aminoacridine, J. Physiol. 483 (Pt 2) (1995) 367–384.
[26] F. Bertaso, et al., Homer1a-dependent crosstalk between NMDA and metabotropic glutamate receptors in mouse neurons, PLoS One 5 (3) (2010) e9755.
[27] H. Wang, et al., Gating mechanism and a modulatory niche of human GluN1-GluN2A NMDA receptors, Neuron 109 (15) (2021) 2443–2456 e5.
[28] A.S. Zhigulin, O.I. Barygin, Mechanisms of NMDA receptor inhibition by sepimostat-comparison with nafamostat and diarylamidine compounds, Int. J. Mol. Sci. 24 (21) (2023).
[29] R. Eckert, D. Ewald, Inactivation of calcium conductance characterized by tail current measurements in neurones of Aplysia californica, J. Physiol. 345 (1983) 549–565.
[30] H. Satoh, J. Hasegawa, M. Vassalle, On the characteristics of the inward tail current induced by calcium overload, J. Mol. Cell. Cardiol. 21 (1) (1989) 5–20.
[31] J.R. Clay, Slow inactivation and reactivation of the K+ channel in squid axons. A tail current analysis, Biophys. J. 55 (3) (1989) 407–414.
[32] H.Y. Jung, N.P. Staff, N. Spruston, Action potential bursting in subicular pyramidal neurons is driven by a calcium tail current, J. Neurosci. 21 (10) (2001) 3312–3321.
[33] V. Libri, et al., Metabotropic glutamate receptor subtypes mediating slow inward tail current (IADP) induction and inhibition of synaptic transmission in olfactory cortical neurones, Br. J. Pharmacol. 120 (6) (1997) 1083–1095.
[34] J. Kiehn, et al., Molecular physiology and pharmacology of HERG. Single-channel currents and block by dofetilide, Circulation 94 (10) (1996) 2572–2579.
[35] A. Dawydow, et al., Channelrhodopsin-2-XXL, a powerful optogenetic tool for low-light applications, Proc. Natl. Acad. Sci. U.S.A. 111 (38) (2014) 13972–13977.
[36] X. Duan, G. Nagel, S. Gao, Mutated channelrhodopsins with increased sodium and calcium permeability, Appl. Sci. 9 (4) (2019) 664.
[37] T. Ruijing, Optogenetic Methods to Regulate Water Transport and Purify Proteins, 2021.
[38] G. Alexander, Characterisation and Application of New Optogenetic Tools in Drosophila melanogaster, 2019.
[39] P. Volz, et al., Light and pH-induced changes in structure and accessibility of transmembrane helix B and its immediate environment in channelrhodopsin-2, J. Biol. Chem. 291 (33) (2016) 17382–17393.
[40] S. Hososhima, et al., Kinetic evaluation of photosensitivity in bi-stable variants of chimeric channelrhodopsins, PLoS One 10 (3) (2015) e0119558.
[41] J. Mattis, et al., Principles for applying optogenetic tools derived from direct comparative analysis of microbial opsins, Nat. Methods 9 (2) (2011) 159–172.
[42] T.E. Chater, et al., Voltage- and temperature-dependent gating of heterologously expressed channelrhodopsin-2, J. Neurosci. Methods 193 (1) (2010) 7–13.
[43] J.Y. Lin, et al., Characterization of engineered channelrhodopsin variants with improved properties and kinetics, Biophys. J. 96 (5) (2009) 1803–1814.
[44] K. Feldbauer, et al., Channelrhodopsin-2 is a leaky proton pump, Proc. Natl. Acad. Sci. U.S.A. 106 (30) (2009) 12317–12322.
[45] E.G. Govorunova, et al., Kalium channelrhodopsins are natural light-gated potassium channels that mediate optogenetic inhibition, Nat. Neurosci. 25 (7) (2022) 967–974.

[46] O. Alvarez, C. Gonzalez, R. Latorre, Counting channels: a tutorial guide on ion channel fluctuation analysis, Adv. Physiol. Educ. 26 (1–4) (2002) 327–341.
[47] D. Zimmermann, et al., Effects on capacitance by overexpression of membrane proteins, Biochem. Biophys. Res. Commun. 369 (4) (2008) 1022–1026.
[48] M.A. Dreier, et al., Time-resolved spectroscopic and electrophysiological data reveal insights in the gating mechanism of anion channelrhodopsin, Commun. Biol. 4 (1) (2021) 578.
[49] V.A. Lorenz-Fonfria, et al., Temporal evolution of helix hydration in a light-gated ion channel correlates with ion conductance, Proc. Natl. Acad. Sci. U.S.A. 112 (43) (2015) E5796–E5804.
[50] V. Haikala, et al., Optogenetic control of fly optomotor responses, J. Neurosci. 33 (34) (2013) 13927–13934.
[51] Z. Zhou, D.M. Bers, Ca2+ influx via the L-type Ca2+ channel during tail current and above current reversal potential in ferret ventricular myocytes, J. Physiol. 523 (Pt 1) (2000) 57–66.
[52] Z.H. Pan, et al., ChR2 mutants at L132 and T159 with improved operational light sensitivity for vision restoration, PLoS One 9 (6) (2014) e98924.
[53] F.J. Sigworth, The variance of sodium current fluctuations at the node of Ranvier, J. Physiol. 307 (1980) 97–129.